

A First Look at the Performance Enhancement Potential of Fluid Reconfigurable Intelligent Surface

Abdelhamid Salem, *Member, IEEE*, Kai-Kit Wong, *Fellow, IEEE*,
George Alexandropoulos, *Senior Member, IEEE*, Chan-Byoung Chae, *Fellow, IEEE*, and
Ross Murch, *Fellow, IEEE*

Abstract—The fluid antenna concept represents shape-flexible and position-flexible antenna technologies designed to enhance wireless communication applications. In this paper, we apply this concept to reconfigurable intelligent surfaces (RISs), introducing fluid RIS (FRIS), where each tunably reflecting element becomes a fluid element with additional position reconfigurability. This new paradigm is referred to as fluid RIS (FRIS). We investigate an FRIS-programmable wireless channel, where the fluid metasurface is divided into non-overlapping subareas, each acting as a fluid element that can dynamically adjust both its position and phase shift of the reflected signal. We first analyze the single-user, single-input single-output (SU-SISO) channel, in which a single-antenna transmitter communicates with a single-antenna receiver via an FRIS. The achievable rate is maximized by optimizing the fluid elements using a particle swarm optimization (PSO)-based approach. Next, we extend our analysis to the multi-user, multiple-input single-output (MU-MISO) case, where a multi-antenna base station (BS) transmits individual data streams to multiple single-antenna users via an FRIS. In this case, the joint optimization of the positions and phase shifts of the FRIS element, as well as the BS precoding to maximize the sum-rate is studied. To solve the problem, a combination of techniques including PSO, semi-definite relaxation (SDR), and minimum mean square error (MMSE) is proposed. Numerical results demonstrate that the proposed FRIS approach significantly outperforms conventional RIS configurations in terms of achievable rate performance.

Index Terms—Fluid antenna system (FAS), movable antenna, particle swarm optimization, programmable metasurface, reconfigurable antenna, reconfigurable intelligent surface (RIS).

I. INTRODUCTION

IN recent years, the technology of reconfigurable intelligent surfaces (RISs) has become the center of research in wireless communications. This is because it promises to

The work of A. Salem and K.-K. Wong was supported by the Engineering and Physical Sciences Research Council (EPSRC) under Grant EP/W026813/1. The work of C.-B. Chae This work was also supported by IITP (IITP-2025-RS-2024-00428780, IITP-2021-0-00486) grants funded by the Korean government. The work of R. Murch was supported by the Hong Kong Research Grants Council Area of Excellence grant AoE/E-601/22-R.

A. salem and K.-K. Wong are with the Department of Electronic and Electrical Engineering, University College London, London, United Kingdom. K.-K. Wong is also with Yonsei Frontier Lab, Yonsei University, Seoul, Korea (e-mails: {a.salem, kai-kit.wong}@ucl.ac.uk). A. Salem is also affiliated with Benghazi University, Benghazi, Libya.

G. C. Alexandropoulos is with the Department of Informatics and Telecommunications, National and Kapodistrian University of Athens, 16122 Athens, Greece and the Department of Electrical and Computer Engineering, University of Illinois Chicago, IL 60601, USA (e-mail: alexandg@di.uoa.gr)

C.-B. Chae is with the School of Integrated Technology, Yonsei University, Seoul, 03722, Korea (e-mail: cbchae@yonsei.ac.kr).

R. Murch is with the Department of Electronic and Computer Engineering and Institute for Advanced Study (IAS), The Hong Kong University of Science and Technology, Clear Water Bay, Hong Kong SAR, China (e-mail: eermurch@ust.hk).

Corresponding author: Kai-Kit Wong.

enhance coverage of small base stations (BSs) in the sixth generation (6G) of wireless networks when the direct links can be severely weakened or blocked, a situation that can often happen when increasing the carrier frequency [1], [2], [3]. An RIS is a flat surface consisting of a large number of metamaterials with dynamically tunable responses over the impinging signals. By controlling the phase responses of the elements, RISs can intelligently reflect signals and hence have the ability to engineer the propagation environment that benefits many wireless applications [4]. RISs are supposed to be of low power consumption comprising almost passive tunably reflecting elements, though recent trend also investigates the use of semi-passive [5], [6] and active [7], [8], [9] RISs.

Despite the prospect of RIS, practical applications do face certain challenges. To unleash the power of RISs, the complexity of channel estimation must be overcome and is challenging as it involves the incoming and outgoing channels [10], [11], [12], and the computational power of an RIS is supposed to be low. Besides, the phase shifting resolution of the elements is often limited to keep the cost down [4], which complicates the optimization and reduces the degrees-of-freedom (DoF) [13], [14]. The use of RISs in multi-band situations is also messy since it has dissimilar responses at different frequencies [15]. Recently, [16], [17] examined the power consumption of RISs with practical models, with the latter work providing an experimental validation. Overall, a lot of issues around RISs have to do with whether the performance gain justifies the cost. It would be appealing if we could obtain higher DoF without the need for raising the number of RIS elements, since this scaling links to the associated cost, control overhead [18], and overall complexity.

In terms of DoF, recent interest has witnessed efforts taking advantage of a new form of reconfigurable antennas, referred to as a fluid antenna system (FAS), to enhance the DoF in the physical layer of wireless communications [19], [20]. In short, FAS represents the antenna technology of shape and position reconfigurability which is motivated by flexible structures, such as liquid-based antennas [21], [22] and liquid-metal metasurfaces [23], movable arrays [24], [25], metamaterial-based antennas [26], [27], [28], pixel reconfigurable antennas [29], [30], etc. The latter two designs are particularly useful as their reconfigurability comes with no delay.

The concept of FAS was first introduced by Wong *et al.* in 2020 [31], [32] which hypothesized a wireless communication system with a position-flexible FAS receiver. Since then, much effort has been made to understand the various performance limits of FAS channels, e.g., [33], [34], [35], [36], [37], [38]. A recent study has also investigated the diversity-multiplexing

tradeoff of a multiple-input multiple-output (MIMO) channel with fluid antennas at both ends [39]. Evidently, channel state information (CSI) is essential to enable FAS and several CSI estimation schemes for FAS have recently been proposed [40], [41], [42], [43]. Position optimization (i.e., port selection) [44] and jointly with beamforming have also become an important technology for many applications, e.g., [45], [46], [47], [48].

An interesting development also sees FAS being employed for multiple access, referred to as fluid antenna multiple access (FAMA). The idea is that interference can be mitigated at the receiver side by activating the position where the interference signal suffers from a deep fade due to multipath propagation. Following this idea, different forms of FAMA techniques have been proposed, including fast [49], [50], slow switching [51] and with coding [52]. Port selection with some analog signal combining has also been considered to improve interference immunity [53], [54]. Opportunistic scheduling and FAMA also can work together to support a good number of users without precoding at the BS nor interference cancellation [55].

Inspired by the position reconfigurability of FAS, we propose in this paper to apply this concept to RISs. Our proposal is also motivated by the fact that an RIS is usually not space-limited, but the number of its elements has to be limited due to complexity reasons. One lesson FAS has taught the wireless communications community is that spatial diversity originates from the space dimension and can be obtained by a *single* ‘fluid’ element.¹ Motivated by this FAS property, this paper proposes a new paradigm, referred to as fluid RIS (FRIS), in which the radiating surface area is divided by non-overlapping subareas, each of which is equipped with a fluid element that can freely appear in any point of the designated subarea, and can reflect the incident signal with an optimized phase shift. This architecture can fully utilize the permissible area without having to install more elements accordingly.

To shed light on the potential of FRIS, we first investigate the single-user single-input single-output (SU-SISO) scenario where a transmitter with a single fixed-position antenna (FPA) communicates to a receiver with an FPA via an FRIS. Assuming that the direct link is broken, we find the optimal positions of the FRIS elements by an approach based on particle swarm optimization. Then, we extend our study to FRIS-aided multi-user multiple-input single-output (MU-MISO) systems in which a multi-FPA BS transmits to multiple users each equipped with an FPA via an FRIS. In this case, we solve the joint optimization problem of the FRIS element positions, their phase shifts, and the BS precoding, assuming the absence of a direct link. It is worth pointing out that FRIS was first proposed in [57] where integrated sensing and communication (ISAC) was considered. The limitation of [57] is however that the work was based on line-of-sight (LoS) only channels, which is not diffidently general. Our main contributions are summarized as follows:

- We obtain an optimized FRIS design for SU-SISO communications utilizing a PSO-based approach to determine the optimal positions of FRIS elements. In our system model, each fluid element is restricted to one subarea to strike a balance between DoF and practicality.
- Additionally, we propose a comprehensive framework for the joint optimization of the FRIS element positions, their phase shifts, and the BS precoding to maximize the sum-rate performance of MU-MISO systems. Specifically, a grid search and a PSO-based approach are developed to find the optimal positions of the FRIS elements in each subarea. Then, for the selected positions, the FRIS phase shifts are obtained by using the semi-definite relaxation (SDR) technique. After that, the minimum mean square error (MMSE) scheme is employed to design the precoder at the BS side.
- We evaluate the impact of various system parameters, such as the transmit signal-to-noise ratio (SNR), and the number of FRIS elements on the achievable rates. Our results demonstrate the significant performance improvements of FRIS-aided communication systems in both SU-SISO and MU-MISO scenarios compared to that using conventional RIS configurations.

The remainder of the paper is organized as follows: Section II introduces the system model of SU-SISO and MU-MISO with the aid of FRIS. The problem formulation and proposed algorithms are given in Section III. Then Section IV provides the numerical results and evaluates the proposed algorithms. Finally, we conclude the paper in Section V.

II. SYSTEM MODEL

In this paper, we consider two system models namely SU-SISO and MU-MISO. Both involve a transmitter needing a RIS to reestablish the communication channel to the receiver(s). In SU-SISO, the transmitter has a single FPA and there is only one user as receiver, while for the MU-MISO model depicted in Fig. 1, the BS transmitter is equipped with multiple FPAs, aiming to communicate to many single-FPA users. For both cases, the direct link between the sender and receiver(s) is assumed broken and the use of RIS is necessary.

For the FRIS, its entire radiating area ($A \times A$ in m^2) is divided into N non-overlapping subareas with no gaps. Each subarea is occupied by a fluid element, so the FRIS has totally N fluid elements.² We use \mathcal{S}_n to denote the set of all (x, y) -coordinates within the subarea of the n -th fluid element. The n -th fluid element is capable of switching to one of L preset positions within \mathcal{S}_n and we denote the position vector of the n -th fluid element by $\mathbf{t}_n = (x_n, y_n)^T$ in which T is the transpose operator. In other words, \mathbf{t}_n dictates the point of reflection of the incident signal in \mathcal{S}_n . As in a typical RIS, the n -th fluid element will impose a phase shift $\angle\theta_n$ on the reflected signal. For convenience, we denote the positions of all the FRIS elements by $\mathbf{t} = [\mathbf{t}_1, \dots, \mathbf{t}_N]$ and their phase shifts by $\Theta = \text{diag}(\boldsymbol{\theta})$ with $\boldsymbol{\theta} = [\theta_1, \dots, \theta_N]^T$.

²Although the FRIS is planar and two-dimensional, we will use an one-dimensional numbering for the elements to simplify our notation.

¹By ‘fluid’ element, we mean that each RIS element has position reconfigurability in addition to phase control for the reflected signal. In a broader sense, however, a fluid element can also exhibit other types of reconfigurability, such as shape and size, as defined within the FAS framework. Thus, our FRIS is more general than RISs based on liquid metals, where shape modification is used to achieve different reflection states [56].

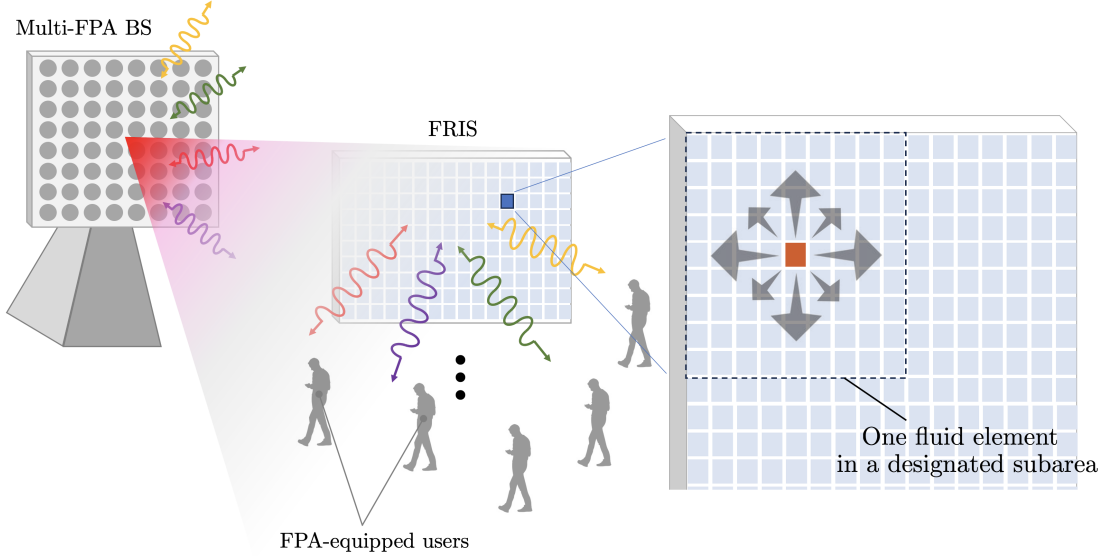


Fig. 1. Illustration of the MU-MISO system assisted by an FRIS.

The model of our fluid element could be interpreted as an ideal movable point reflector, without considering the actual hardware, but in practice, this is more suitably realized using metamaterial-based and reconfigurable pixel technologies for their fast responses and much lower power consumption. For example, the slot-based technology in [58] can be used.

A. SU-SISO

For the case of FRIS-assisted SU-SISO, the received signal at the user can be written as

$$y = \sqrt{P} \mathbf{g}^H \Theta \mathbf{h} s + \eta, \quad (1)$$

where $\mathbf{h} \in \mathbb{C}^{N \times 1}$ is the channel between the transmitter and FRIS, $\mathbf{g} \in \mathbb{C}^{N \times 1}$ is the channel between the FRIS and user, s denotes the information-bearing signal with unit variance, P is the transmit power of the BS, η denotes the additive white Gaussian noise (AWGN) at the user, i.e., $\eta \sim \mathcal{CN}(0, \sigma^2)$, and the superscript H is the Hermitian operator. For the phase shifting matrix $\Theta \in \mathbb{C}^{N \times N}$, we have $\theta_n = e^{j\phi_n}$, where $\phi_n \in [0, 2\pi)$ is the phase shift of element n , and it is assumed that $|\theta_n| = 1 \forall n$. As a result, the received SNR is given by

$$\gamma = \frac{P |\mathbf{g}^H \Theta \mathbf{h}|^2}{\sigma^2}. \quad (2)$$

B. MU-MISO

If the BS is equipped with multiple FPAs and communicates to multiple users in the downlink, then the SU-SISO model becomes the MU-MISO model. Now, assuming that there are M FPAs at the BS and K users, the received signal at the k -th user can be expressed as

$$\begin{aligned} y_k &= \mathbf{g}_k^H \Theta \mathbf{H} \mathbf{W} \mathbf{s} + \eta_k, \\ &= \mathbf{g}_k^H \Theta \mathbf{H} \sum_{\ell=1}^K \mathbf{w}_\ell s_\ell + \eta_k, \end{aligned} \quad (3)$$

where $\mathbf{s} = [s_1 \cdots s_K]^T$ with s_ℓ being the information signal for user ℓ , η_k denotes the AWGN at user k defined similarly as before, $\mathbf{g}_k \in \mathbb{C}^{N \times 1}$ is the channel between the FRIS and user k , $\mathbf{H} \in \mathbb{C}^{N \times M}$ denotes the channel matrix from the BS and FRIS, and $\mathbf{w}_\ell \in \mathbb{C}^{M \times 1}$ is the BS precoding for user ℓ . We also define $\mathbf{W} \triangleq [\mathbf{w}_1 \mathbf{w}_2 \cdots \mathbf{w}_K] \in \mathbb{C}^{M \times K}$ as the overall precoding matrix of the BS. As such, the received signal-to-interference plus noise ratio (SINR) at user k is found as

$$\gamma_k = \frac{P |\mathbf{g}_k^H \Theta \mathbf{H} \mathbf{w}_k|^2}{P \sum_{\ell \neq k}^K |\mathbf{g}_k^H \Theta \mathbf{H} \mathbf{w}_\ell|^2 + \sigma^2}. \quad (4)$$

For convenience, we also define $\mathbf{G} \triangleq [\mathbf{g}_1 \cdots \mathbf{g}_K]$.

C. Channel Model

Here, we discuss how the channels are modelled. We focus on the channel matrices, \mathbf{H} and \mathbf{G} , in the MU-MISO case since \mathbf{h} and \mathbf{g} in the SU-SISO case can be easily deduced from them. In the application of RIS, it is appropriate to model the channel between the BS and FRIS and that between the FRIS and users by Rician fading channels. Specifically, we have

$$\mathbf{H} = \sqrt{l_b} \left(\sqrt{\frac{\rho_b}{\rho_b + 1}} \bar{\mathbf{H}} + \sqrt{\frac{1}{\rho_b + 1}} \tilde{\mathbf{H}} \right), \quad (5)$$

$$\mathbf{g}_k = \sqrt{l_k} \left(\sqrt{\frac{\rho_k}{\rho_k + 1}} \bar{\mathbf{g}}_k + \sqrt{\frac{1}{\rho_k + 1}} \tilde{\mathbf{g}}_k \right), \quad (6)$$

where l_b and l_k represent the path loss scaling factor between the BS and FRIS and that between the FRIS and user k , ρ_b and ρ_k are the Rician factors, $\bar{\mathbf{H}}$ and $\bar{\mathbf{g}}_k$ are the LoS components while $\tilde{\mathbf{H}}$ and $\tilde{\mathbf{g}}_k$ are the non-LoS (NLoS) components.

To characterize how the channel matrices change according to the positions of the elements at the FRIS, \mathbf{t} , we first consider the LoS components of the channels which are modelled as a function of the azimuth and elevation angle-of-departure (AoD) and angle-of-arrival (AoA) as

$$\bar{\mathbf{H}} = \mathbf{a}_r(\phi_r^a, \phi_r^e, \mathbf{t}) \mathbf{a}_t^H(\phi_t), \quad (7)$$

where ϕ_t is the AoD from the BS and $\mathbf{a}_t(\cdot)$ is the BS transmit steering vector with

$$[\mathbf{a}_t(\phi_t)]_m = e^{j(m-1)\pi \sin \phi_t}, \quad (8)$$

where $[\cdot]_m$ returns the m -th entry of the input vector. Similarly, ϕ_r^a and ϕ_r^e represent, respectively, the azimuth AoA and the elevation AoA at the FRIS, and $\mathbf{a}_r(\cdot)$ is the receive steering vector at the FRIS with

$$[\mathbf{a}_r(\phi_r^a, \phi_r^e, \mathbf{t})]_n = e^{j\frac{2\pi}{\lambda}(x_n \sin \phi_r^a \cos \phi_r^e + y_n \sin \phi_r^e)} \quad (9)$$

with λ being the carrier wavelength. For the FRIS to user k 's channel, we also have

$$\bar{\mathbf{g}}_k = \mathbf{a}(\phi_k^a, \phi_k^e, \mathbf{t}), \quad (10)$$

where ϕ_k^a and ϕ_k^e are, respectively, the azimuth and elevation AoD from the FRIS to user k , and $\mathbf{a}(\cdot)$ is the transmit steering vector of the FRIS to user k with

$$[\mathbf{a}(\phi_k^a, \phi_k^e, \mathbf{t})]_n = e^{j\frac{2\pi}{\lambda}(x_n \sin \phi_k^a \cos \phi_k^e + y_n \sin \phi_k^e)}. \quad (11)$$

For the NLoS components, we model the spatial correlation of the channels using Jake's model. Let us define \mathbf{J}_b and \mathbf{J}_k as the spatial correlation matrices for the BS-FRIS and FRIS-user k channels, respectively. Then we have

$$[\mathbf{J}_b]_{i,j} = J_0\left(\frac{2\pi\Delta d_{i,j}}{\lambda}\right), \quad (12)$$

$$[\mathbf{J}_k]_{m,n} = J_0\left(\frac{2\pi\Delta d_{m,n}}{\lambda}\right) \quad (13)$$

where $J_0(\cdot)$ denotes the zeroth-order Bessel function of the first kind, and $\Delta d_{i,j}$ and $\Delta d_{m,n}$ denote the distances between the i -th and j -th FRIS elements of the BS-FRIS channel, and between the m -th and n -th FRIS elements of the FRIS-user k channel, respectively. Specifically, the spatial correlation matrices \mathbf{J}_b and \mathbf{J}_k can be decomposed as

$$\mathbf{J}_b = \mathbf{U}_b \mathbf{\Lambda}_b \mathbf{U}_b^H, \quad (14)$$

$$\mathbf{J}_k = \mathbf{U}_k \mathbf{\Lambda}_k \mathbf{U}_k^H, \quad (15)$$

where \mathbf{U}_b and \mathbf{U}_k are unitary matrices containing the eigenvectors of the correlation matrices, and $\mathbf{\Lambda}_b$ and $\mathbf{\Lambda}_k$ are diagonal matrices containing the eigenvalues. Thus, the mathematical expressions of the NLoS channel matrix $\tilde{\mathbf{H}}$ and the channel vector $\tilde{\mathbf{g}}_k$ can be expressed as

$$\tilde{\mathbf{H}} = \mathbf{\Lambda}_b^{1/2} \mathbf{U}_b^H \hat{\mathbf{H}}, \quad (16)$$

$$\tilde{\mathbf{g}}_k = \mathbf{\Lambda}_k^{1/2} \mathbf{U}_k^H \hat{\mathbf{g}}_k, \quad (17)$$

where $\hat{\mathbf{H}}$ and $\hat{\mathbf{g}}_k$ represent the uncorrelated small-scale fading components, with their elements modelled as independent and identically distributed (i.i.d.) complex Gaussian distributions with zero mean and unit variance.

III. MAIN RESULTS

In this section, we present the problem formulations of both models and attempt to optimize the FRIS for performance enhancement. Specifically, our interest is on maximizing the achievable rate of the system given some constraints.

A. SU-SISO

First, the SU-SISO model is considered. Assuming capacity-achieving codec is being adopted, the achievable rate depends only on the SNR. Our objective is to maximize the achievable rate by optimizing the FRIS elements. That is,

$$\max_{\mathbf{t}, \Theta} \log_2 \left(1 + \frac{P |\mathbf{g}^H \Theta \mathbf{h}|^2}{\sigma^2} \right) \quad (18a)$$

$$\text{s.t. } \mathbf{t}_n \in \mathcal{S}_n, \forall n \quad (18b)$$

$$\|\mathbf{t}_n - \mathbf{t}_{n'}\|_2 \geq D, \forall n \neq n' \quad (18c)$$

$$|\theta_n| = 1, \forall n, \quad (18d)$$

in which \mathcal{S}_n is the feasible subarea for the n -th fluid element to roam and D denotes a minimum spacing set between two fluid elements. Depending on what technology the fluid element is based on, the value of D could have a different interpretation. For example, if mechanically movable radiating elements are employed, then D will play a key role to control the level of mutual coupling between the adjacent elements.³ By contrast, D would be much less meaningful if other technologies such as metamaterials or reconfigurable pixels are considered.

To solve (18), it is clear that the optimal phase shift of each fluid element is to cancel the overall phase shift imposed by the first- and second-hop channels, i.e.,

$$\theta_n^* = e^{-j(\angle[\mathbf{h}]_n + \angle[\mathbf{g}]_n)}. \quad (19)$$

Hence, the optimization problem (18) can be reduced to

$$\max_{\mathbf{t}} \log_2 \left(1 + \frac{P \left| \sum_{n=1}^N \|\mathbf{h}_n\| \|\mathbf{g}_n\| \right|^2}{\sigma^2} \right) \quad (20a)$$

$$\text{s.t. } \mathbf{t}_n \in \mathcal{S}_n, \forall n \quad (20b)$$

$$\|\mathbf{t}_n - \mathbf{t}_{n'}\|_2 \geq D, \forall n \neq n'. \quad (20c)$$

The problem is inherently non-convex and computationally intensive due to the high-dimensional search space. Evaluating all the possible combinations of the fluid element positions by adopting an exhaustive search algorithm or greedy algorithm is prohibitively complex, especially when the number of fluid elements grows large. To efficiently overcome this challenge, a PSO-based algorithm is proposed. PSO can converge quickly to near-optimal solutions without requiring derivative information. Moreover, it can incorporate subarea boundaries and minimum spacing between elements into the optimization, ensuring feasible and deployable solutions. PSO is an efficient choice for optimizing FRIS due to its efficiency in handling high-dimensional, non-convex, and combinatorial problems. Unlike exhaustive search, which is computationally prohibitive, PSO leverages swarm intelligence to explore the solution space effectively while avoiding local optima. Compared to gradient-based methods, which struggle with non-differentiable constraints, and alternative metaheuristics like genetic algorithms and simulated annealing, which often

³Note that mutual coupling is not always harmful as observed in [54] as far as beamforming is concerned. Even if the aim is to minimize mutual coupling, state-of-the-art technologies can already reduce it to a very low level even if the separation is as little as 0.1λ where λ is the carrier wavelength [59], [60].

exhibit slower convergence, PSO provides a balance between global exploration and local refinement. Its ability to incorporate spatial constraints ensures practical deployment, while its fast convergence and computational efficiency enable near-optimal solutions in real-time wireless scenarios.

In our model, the area of FRIS is divided into N subareas, each assigned to one fluid element. Each subarea is defined by some boundary. For the n -th subarea, it is defined by the ranges $[x_{\min}^n, x_{\max}^n]$ and $[y_{\min}^n, y_{\max}^n]$ in the x - and y -axis, respectively. The distance between any two subareas should satisfy the constraint (20c). The optimization within each subarea is conducted independently using PSO. In the PSO-based algorithm, we first randomly initialize particles with the positions and velocities. Then we calculate the fitness of each particle based on the objective function. Each particle updates its position based on the individual experience (the currently known local best-position, $\mathbf{t}_{i,\text{best}}$) and the swarm experience (the currently known global best position, \mathbf{t}_{best}). Consequently, the velocity of each particle is updated by

$$\mathbf{v}_i^{(t+1)} = \omega \mathbf{v}_i^{(t)} + c_1 r_1 [\mathbf{t}_{i,\text{best}} - \mathbf{t}_i^{(t)}] + c_2 r_2 [\mathbf{t}_{\text{best}} - \mathbf{t}_i^{(t)}], \quad (21)$$

where t is the iteration index, $\mathbf{v}_i^{(t+1)}$ is the new velocity of particle i at iteration $t+1$, ω is the inertia weight to balance the speed and accuracy of particle swarm search, c_1, c_2 are the individual and global learning factors, which represent the step size of each particle moving toward the best position, r_1, r_2 are random numbers between 0 and 1 to enhance the randomness of the search for escaping from local optima. Also, for each iteration, the position of each particle is updated as

$$\mathbf{t}_i^{(t+1)} = \mathcal{P}(\mathbf{t}_i^{(t)} + \mathbf{v}_i^{(t+1)}), \quad (22)$$

where $\mathcal{P}(\cdot)$ is the projection function to enforce the boundary constraint (20b). If a particle moves out of the boundaries of the feasible region, we project its position to the corresponding maximum or minimum value. Also, constraint (20c) is already satisfied after dividing the FRIS area into N disjoint subareas with minimum spacing D . Moreover, we introduce an adaptive penalty factor to the fitness function to guarantee that the constraints are met. Thus, the objective function becomes

$$\mathcal{D}(\mathbf{t}_i^{(t)}) = R(\mathbf{t}_i^{(t)}) - \tau \mathfrak{B}(\mathbf{t}_i^{(t)}), \quad (23)$$

in which $R(\cdot)$ represents the original rate function in (20a), τ is a large positive penalty parameter which ensures that the inequality, $R(\mathbf{t}_i^{(t)}) - \tau \leq 0$ holds for all the positions, meaning that the penalty parameter moves each particle position in order to ensure the minimum spacing constraint, and $\mathfrak{B}(\mathbf{t}_i^{(t)})$ is the penalty function which accounts for the position violation of fluid element i against (20c), defined as

$$\mathfrak{B}(\mathbf{t}) = \{(\mathbf{t}_n, \mathbf{t}_{n'}) \mid \|\mathbf{t}_n - \mathbf{t}_{n'}\|_2 < D, 1 \leq n < n' \leq N\}. \quad (24)$$

The PSO-based algorithm is summarized in Algorithm 1.

B. MU-MISO

In the case of FRIS-aided MU-MISO system, our interest is to maximize the sum-rate of all users in the downlink, which

Algorithm 1 PSO-Based Algorithm

1. Input: Overall FRIS area $[X_{\min}, X_{\max}]$ and $[Y_{\min}, Y_{\max}]$, N , D , PSO parameters.
 2. Divide the FRIS area into N subareas with distance D , each defined by $[x_{\min}^n, x_{\max}^n]$ and $[y_{\min}^n, y_{\max}^n]$.
 3. Pre-compute the channels for each subarea.
 4. For each FRIS element:
 - a. Perform PSO within the subarea:
 - i. Initialize particles and velocities.
 - ii. For each iteration:
 - Evaluate fitness for all particles.
 - Update personal and global best positions.
 - Update particle velocities and positions.
 - Enforce subarea boundaries.
 - iii. Select the optimal position for the element.
 - b. Check minimum spacing constraint (20c) with previously selected positions.
 - c. If spacing constraint is violated:
 - Re-optimize for a valid position.
 - d. Append valid position to selected positions.
 5. Output: selected positions and corresponding rate values.
-

can be formulated as

$$\max_{\mathbf{t}, \boldsymbol{\theta}, \mathbf{w}} \sum_{k=1}^K \log_2 \left(1 + \frac{|\mathbf{g}_k^H \boldsymbol{\Theta} \mathbf{H} \mathbf{w}_k|^2}{\sum_{\substack{\ell=1 \\ \ell \neq k}}^K |\mathbf{g}_k^H \boldsymbol{\Theta} \mathbf{H} \mathbf{w}_\ell|^2 + \sigma^2} \right) \quad (25a)$$

$$\text{s.t. } \mathbf{t}_n \in \mathcal{S}_n, \forall n \quad (25b)$$

$$\|\mathbf{t}_n - \mathbf{t}_{n'}\|_2 \geq D, \forall n \neq n' \quad (25c)$$

$$|\theta_n| = 1, \forall n, \quad (25d)$$

$$\sum_{k=1}^K \|\mathbf{w}_k\|^2 \leq P, \quad (25e)$$

where (25e) is the power constraint which becomes important in the optimization. The other constraints remain the same. An obvious challenge now is to also jointly optimize the precoding matrix at the BS. Problem (25) is very challenging, due to the complexity of the objective function, the modulus constraint, and the non-convex norm form. Given the non-convexity of the problem, we resort to an alternating optimization strategy. In particular, we solve (25) by updating each variable iteratively with the other variables fixed. Now we decouple it into three sub-problems: 1) FRIS Position Optimization, 2) Phase Shift Optimization, and 3) Precoding Optimization.

- 1) *FRIS Position Optimization*—We aim to determine the optimal positions of the fluid elements that maximize the received SINR and improve the overall system performance. The phase shifts and precoder are assumed to be fixed or precomputed based on the current positions. For each fluid element, we consider a set of possible positions within a predefined subarea, and the position that maximizes the sum rate can be selected using PSO, as explained in Section III-A, or by a grid search which systematically evaluates each candidate position within a defined search space. During the grid search, candidate positions that violate the spacing constraint are excluded

from the search. For fluid element n , divide its subarea into a grid with resolution Δx and Δy in both directions, producing a set of candidate positions. For candidate position \mathbf{t}_n , compute the BS-to-FRIS channel $\mathbf{H}^{(n)}$ and the FRIS-to-users channel $\mathbf{G}^{(n)}$. Then compute the sum-rate for each candidate position. For each subarea, select the position \mathbf{t}_n^* that maximizes the sum-rate, i.e.,

$$\mathbf{t}_n^* = \arg \max_{\mathbf{t}_n} \sum_{k=1}^K \log_2 (1 + \text{SINR}_k(\mathbf{t}_n)). \quad (26)$$

PSO is computationally efficient for large search spaces, when the grid search becomes expensive. The key components of PSO to find the optimal positions has been explained in Section III-A.

- 2) *Phase Shift Optimization*—Here we optimize the phase shift matrix Θ to align the reflected signals constructively. Thus, the optimization problem is formulated as

$$\max_{\Theta} \sum_{k=1}^K \log_2 \left(1 + \frac{|\mathbf{g}_k^H \Theta \mathbf{H} \mathbf{w}_k|^2}{\sum_{\substack{\ell=1 \\ \ell \neq k}}^K |\mathbf{g}_k^H \Theta \mathbf{H} \mathbf{w}_\ell|^2 + \sigma^2} \right) \quad (27a)$$

$$\text{s.t. } |\theta_n| = 1, \forall n, \quad (27b)$$

which can be solved using SDR techniques. SDR can efficiently handle the non-convex unit-modulus constraint on the FRIS elements, which makes direct optimization difficult. By lifting the problem into a higher-dimensional space and relaxing the rank-one constraint, SDR transforms it into a convex semi-definite program (SDP) that can be efficiently solved using standard optimization tools. Compared to brute-force or non-linear methods, SDR is computationally efficient and enables iterative refinements for higher spectral efficiency and sum rate. Let us define the effective channel for user k , $\mathbf{h}_{\text{eff},k} = \mathbf{g}_k^H \Theta \mathbf{H}$. Thus, the SINR for user k is reexpressed as

$$\gamma_k = \frac{|\mathbf{h}_{\text{eff},k} \mathbf{w}_k|^2}{\sum_{\substack{\ell=1 \\ \ell \neq k}}^K |\mathbf{h}_{\text{eff},k} \mathbf{w}_\ell|^2 + \sigma^2}. \quad (28)$$

To relax the unit-modulus constraint, we write $\mathbf{v} = [e^{j\phi_1}, \dots, e^{j\phi_N}]^T$, and $\Theta = \text{diag}(\mathbf{v})$, which gives

$$\mathbf{h}_{\text{eff},k} = \mathbf{v}^H \text{diag}(\mathbf{g}_k^H) \mathbf{H} \quad (29)$$

and

$$|\mathbf{h}_{\text{eff},k} \mathbf{w}_k|^2 = \mathbf{v}^H \mathbf{A}_k \mathbf{v}, \quad (30)$$

where $\mathbf{A}_k = \text{diag}(\mathbf{g}_k^H) \mathbf{H} \mathbf{w}_k \mathbf{w}_k^H \mathbf{H}^H \text{diag}(\mathbf{g}_k^H)^H$. Similarly, we get

$$\sum_{j \neq k} |\mathbf{h}_{\text{eff},k} \mathbf{w}_j|^2 = \sum_{j \neq k} \mathbf{v}^H \mathbf{B}_{k,j} \mathbf{v}, \quad (31)$$

in which $\mathbf{B}_{k,j} = \text{diag}(\mathbf{g}_k^H) \mathbf{H} \mathbf{w}_j \mathbf{w}_j^H \mathbf{H}^H \text{diag}(\mathbf{g}_k^H)^H$. The overall SINR term then becomes

$$\gamma_k = \frac{\mathbf{v}^H \mathbf{A}_k \mathbf{v}}{\mathbf{v}^H \mathbf{B}_k \mathbf{v} + \sigma^2}. \quad (32)$$

where $\mathbf{B}_k \triangleq \sum_{j \neq k} \mathbf{B}_{k,j}$. The next step is to replace $\mathbf{v} \mathbf{v}^H$ by a positive semidefinite (PSD) matrix \mathbf{V} , so $\mathbf{V} = \mathbf{v} \mathbf{v}^H$. SDR removes the rank-one constraint, allowing \mathbf{V} to be any PSD matrix, and the solution is projected back to the feasible set. Now we can reformulate the phase shift optimization problem as

$$\max_{\mathbf{V}} \sum_{k=1}^K \log_2 \left(1 + \frac{\text{trace}(\mathbf{A}_k \mathbf{V})}{\text{trace}(\mathbf{B}_k \mathbf{V}) + \sigma^2} \right) \quad (33a)$$

$$\text{s.t. } \mathbf{V} \succeq \mathbf{0}, \quad (33b)$$

$$\text{diag}(\mathbf{V}) = \mathbf{1}. \quad (33c)$$

Then we can replace the fraction inside the logarithm using an alternative transformation. Hence, the objective function can be written as

$$\log_2 (\text{trace}(\mathbf{A}_k \mathbf{V}) + \text{trace}(\mathbf{B}_k \mathbf{V}) + \sigma^2). \quad (34)$$

The relaxed SDP problem can then be written as

$$\max_{\mathbf{V}} \sum_{k=1}^K \log_2 (\text{trace}(\mathbf{A}_k \mathbf{V}) + \text{trace}(\mathbf{B}_k \mathbf{V}) + \sigma^2) \quad (35a)$$

$$\text{s.t. } \mathbf{V} \succeq \mathbf{0}, \quad (35b)$$

$$\text{diag}(\mathbf{V}) = \mathbf{1}. \quad (35c)$$

To proceed further, we approximate (35a) using first-order Taylor series expansion. Before that, we define

$$f_k(\mathbf{V}) \triangleq \text{trace}(\mathbf{A}_k \mathbf{V}) + \text{trace}(\mathbf{B}_k \mathbf{V}) + \sigma^2. \quad (36)$$

By approximating $\log_2(f(\mathbf{V}))$ using first-order Taylor series expansion around a feasible point $\mathbf{V}^{(t-1)}$ (at the previous iteration), we have

$$\log_2(f_k(\mathbf{V})) \approx \log_2(f_k(\mathbf{V}^{(t-1)})) + \frac{1}{\ln 2} \frac{\text{trace}(\mathbf{A}_k \mathbf{V}) + \text{trace}(\mathbf{B}_k \mathbf{V}) - f_k(\mathbf{V}^{(t-1)})}{f_k(\mathbf{V}^{(t-1)})}. \quad (37)$$

This transforms the problem into a convex one that can be solved iteratively. Generally, the relaxed problem may not lead to a rank-one solution, which implies that the optimal objective value of problem can only serve as an upper bound. Additional steps are needed to construct a rank-one solution from the obtained higher-rank solution to the problem. To do so, we extract a feasible solution from \mathbf{V} using eigenvalue decomposition

$$\begin{cases} \mathbf{v} = \sqrt{\lambda_1} \mathbf{u}_1, \\ \mathbf{V} \approx \lambda_1 \mathbf{u}_1 \mathbf{u}_1^H, \end{cases} \quad (38)$$

where λ_1 and \mathbf{u}_1 are the largest eigenvalue and the corresponding eigenvector of \mathbf{V} . The steps of the phase shift optimization are summarized in Algorithm 2.

Algorithm 2 Phase Shift Optimization.

1. Initialize $\mathbf{V}^{(0)}$ with a feasible PSD matrix.
 2. Repeat until convergence:
 - Compute $f_k(\mathbf{V}^{(t-1)})$ for the current iteration.
 - Solve the convex SDP problem.
 - Update $\mathbf{V}^{(t)}$ with the solution from SDR.
 - If $\|\mathbf{V}^{(t)} - \mathbf{V}^{(t-1)}\|$ is small, stop.
 3. Use eigenvalue decomposition (38).
-

- 3) *Precoding Matrix Optimization*—The remaining task is to optimize the precoding matrix \mathbf{W} at the BS, which can be formulated as

$$\max_{\mathbf{W}} \sum_{k=1}^K \log_2 \left(1 + \frac{|\mathbf{g}_k^H \Theta \mathbf{H} \mathbf{w}_k|^2}{\sum_{\substack{\ell=1 \\ \ell \neq k}}^K |\mathbf{g}_k^H \Theta \mathbf{H} \mathbf{w}_\ell|^2 + \sigma^2} \right) \quad (39a)$$

$$\text{s.t.} \quad \sum_{k=1}^K \|\mathbf{w}_k\|^2 \leq P. \quad (39b)$$

To solve this precoding optimization problem, we implement the MMSE technique. MMSE minimizes the total error between the transmitted and received signals, leading to better robustness. It is particularly beneficial in multi-user systems, where interference between users should be mitigated while maximizing the sum rate. Additionally, MMSE is convex and computationally efficient, allowing for real implementation in FRIS-assisted MU-MISO networks. Inspired by the MU-MISO results in [43], we define the mean square error as

$$e_k = 1 - 2\text{Re}\{u_k^* \mathbf{h}_{\text{eff},k} \mathbf{w}_k\} + |u_k|^2 Q_k, \quad (40)$$

where u_k is the complex receiver scaling at user k , $Q_k = \sum_{\substack{\ell=1 \\ \ell \neq k}}^K |\mathbf{g}_k^H \Theta \mathbf{H} \mathbf{w}_\ell|^2 + \sigma^2$ is the total interference-plus-noise power for user k , and

$$\mathbf{h}_{\text{eff},k} \triangleq \mathbf{g}_k^H \Theta \mathbf{H}. \quad (41)$$

Then by introducing the auxiliary optimization variables $\varpi = [\varpi_1, \dots, \varpi_K]^T$, we can reformulate (39) as a more tractable MMSE problem as

$$\min_{\mathbf{W}, \{u_k\}, \varpi} \sum_{k=1}^K (\varpi_k e_k - \log(\varpi_k)) \quad (42a)$$

$$\text{s.t.} \quad \sum_{k=1}^K \|\mathbf{w}_k\|^2 \leq P \quad (42b)$$

$$\varpi_k > 0, \forall k, \quad (42c)$$

which can be solved using an iterative MMSE algorithm below. To do so, first, we optimize u_k for a fixed \mathbf{W} and ϖ , with the optimal solution given by

$$u_k = \frac{\mathbf{h}_{\text{eff},k} \mathbf{w}_k}{Q_k}. \quad (43)$$

Then for fixed \mathbf{W} and $\{u_k\}_{\forall k}$, the optimal auxiliary variable can be found as

$$\varpi_k = \frac{1}{e_k}. \quad (44)$$

Now, for fixed $\{u_k\}_{\forall k}$ and ϖ , the optimal precoder can be obtained by solving

$$\min_{\mathbf{W}} \sum_{k=1}^K \varpi_k [1 - 2\text{Re}\{u_k^* \mathbf{h}_{\text{eff},k} \mathbf{w}_k\} + |u_k|^2 Q_k] \quad (45a)$$

$$\text{s.t.} \quad \sum_{k=1}^K \|\mathbf{w}_k\|^2 \leq P, \quad (45b)$$

which is convex in \mathbf{W} and can therefore be solved using standard convex optimization tools (e.g., CVX). As such, we have Algorithm 3 to solve (39).

Algorithm 3 Proposed Algorithm for BS Precoding.

1. Generate possible positions \mathbf{t} for each fluid element.
 2. Precompute BS-to-FRIS and FRIS-to-user channels \mathbf{H} and \mathbf{G} for all possible positions.
 3. For each FRIS element, select the position using (26).
 4. Use Algorithm 2 to obtain optimal phase shifts of the selected positions.
 5. Use MMSE Algorithm to obtain \mathbf{W} .
 6. Repeat Step 3 until convergence in the sum-rate.
-

C. Complexity and Convergence Analysis

The complexity of FRIS optimization with N fluid elements and \mathcal{N} candidate positions in each subarea is $O(N \cdot \mathcal{N})$. The complexity of phase shift optimization using SDR is $O(N^3)$ per iteration, and the complexity of precoding optimization using MMSE is $O(M^3 + M^2 K)$ per iteration. Therefore, the overall complexity per iteration is $O(K \cdot N^3 + M^3)$.

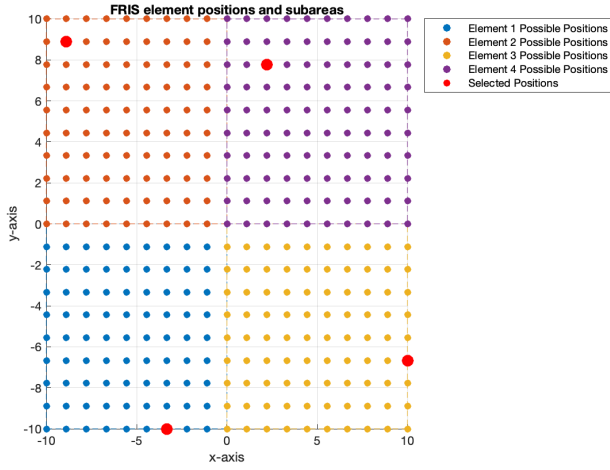
The FRIS position optimization converges in a few steps due to grid search, and the phase shift optimization using SDR converges to a solution satisfying the relaxed constraints. In addition, the precoding optimization using MMSE converges due to the convexity of sub-problems. The overall objective (sum-rate) is non-decreasing and upper-bounded.

IV. NUMERICAL RESULTS AND DISCUSSION

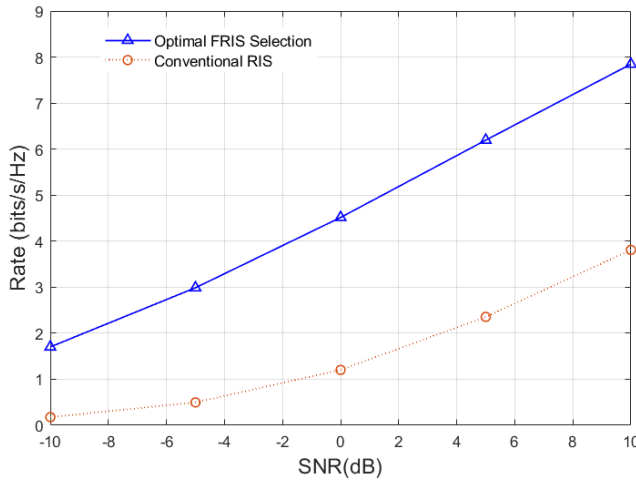
In this section, simulation results are provided to assess the rate performance of the proposed FRIS-assisted systems and compare that with the conventional RIS counterpart. In the simulations, we consider the locations of the BS and FRIS at $(0, 0)$ and $(20, 20)$ in meters, respectively, while the users are distributed in a circle centered at $(20, 0)$ meters with radius of 10 m. The minimal element spacing is $D = \lambda/2$, and the size of FRIS/RIS is $A \times A$ where $A = 4$ m unless otherwise specified. The wavelength of $\lambda = 0.125$ m is set and thus the carrier frequency is 2.4 GHz. Moreover, for the case of MU-MISO, we have $M = 8$ BS antennas and $K = 4$ users. Additionally, the path-loss exponent is set to 2.7, and the Rician factor is 3. The AoA and AoD of the BS and FRIS are randomly and uniformly distributed in $(0, \pi)$.

A. SU-SISO

We first examine the performance in the case of SU-SISO systems with the aid of FRIS. The rate performance results are



(a) Optimal elements positions

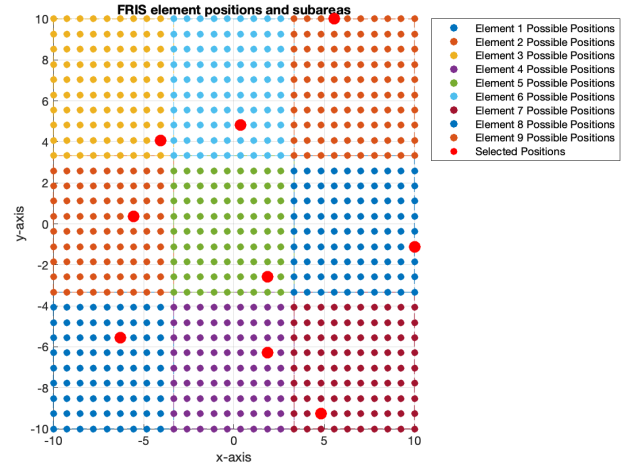


(b) Rate performance

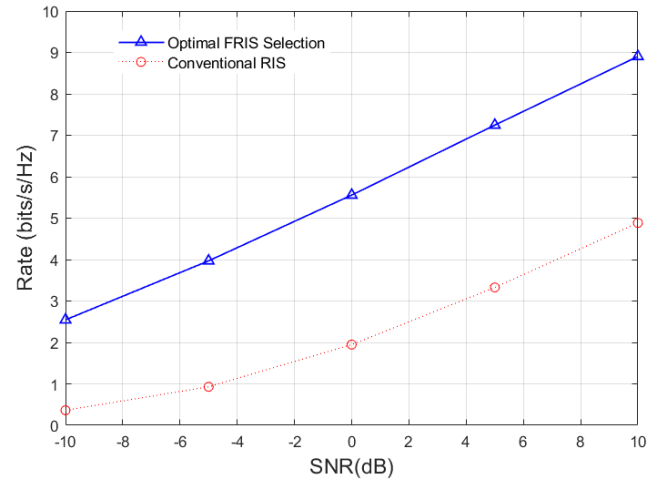
Fig. 2. Comparison between the proposed FRIS-aided SU-SISO and conventional RIS systems when $N = 4$.

provided in Figs. 2–4 for $N = 4, 9, 16$, respectively. Fig. 2(a) illustrate the possible fluid element positions on FRIS in the simulations when there are only $N = 4$ fluid elements. In that figure, an example of the best fluid element positions is also shown. As can be seen, the optimized positions indicate strategic positioning in the subareas for performance enhancement. Evidently, the exact relationship between the achievable rate and the fluid element positions is complicated and depends on the instantaneous channels.

The results in Figs. 2(b), 3(b) and 4(b) demonstrate promising rate performance for using FRIS compared to the conventional RIS systems. As expected, the achievable rates in all the cases increase with the number of elements and the SNR. More importantly, significant rate increase is observed utilizing the proposed FRIS system. Specifically, at 10 dB of SNR, a rate increase from 4 bits/s/Hz to 8 bits/s/Hz is achieved when $N = 4$. Similar gains are consistently observed when $N = 9$, from 6.5 bits/s/Hz to 9.5 bits/s/Hz, and $N = 16$, from 7.5 bits/s/Hz to 10.5 bits/s/Hz over conventional RIS systems.



(a) Optimal elements positions



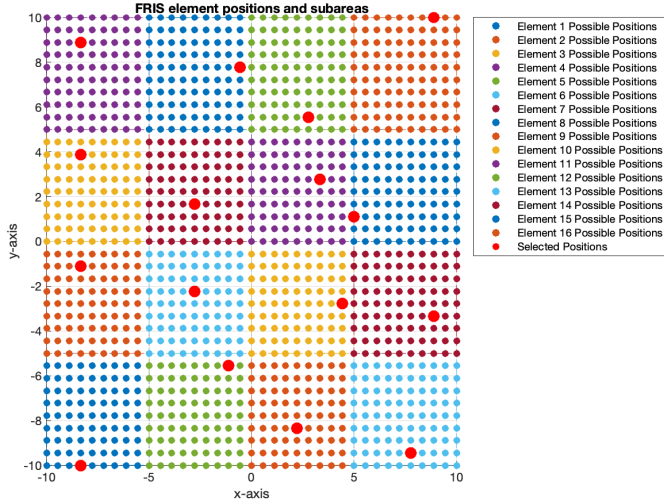
(b) Rate performance

Fig. 3. Comparison between the proposed FRIS-aided SU-SISO and conventional RIS systems when $N = 9$.

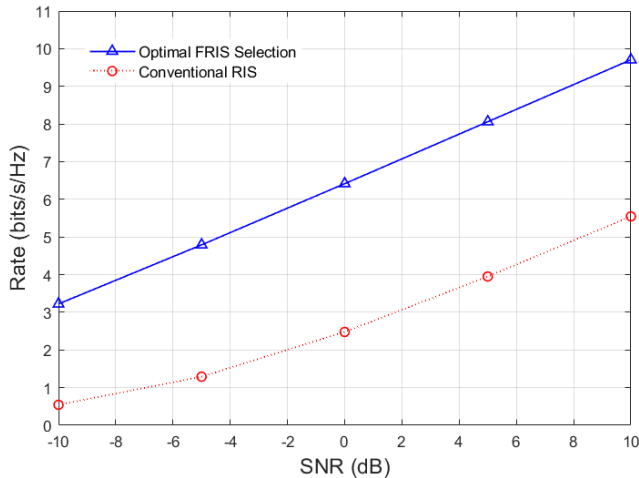
In Fig. 5, we investigate the convergence performance of Algorithm 1 for the optimization of fluid element positioning using the PSO-based method. In the simulations, 10 dB SNR is assumed and different values of N are considered. The results in this figure show that the proposed PSO-based algorithm converges quickly although more iterations would be required if more fluid elements are involved. Decent performance after 10 or 20 iterations before convergence can be obtained.

B. MU-MISO

In this subsection, we turn our attention to the MU-MISO setup in which multiple users are considered and the BS has multiple FPAs for precoding. The rate performance results for the FRIS-aided MU-MISO system are provided in Fig. 6 for different values of fluid elements, N , while the candidate positions for the fluid elements are the same as the case of SU-SISO before and thus omitted. In the multi-user case, the sum-rate performance is considered, and the BS precoding is optimized together with the fluid element positioning. First of



(a) Optimal elements positions



(b) Rate performance

Fig. 4. Comparison between the proposed FRIS-aided SU-SISO and conventional RIS systems when $N = 16$.

all, it is expected that the rate increases with the number of elements and SNR. Also, FRIS continues to outperform clearly the conventional RIS counterpart, demonstrating the good use of spatial diversity in position reconfigurability of the fluid elements. However, one interesting observation is regarding FRIS with $N = 4$ and conventional RIS with $N = 16$. At SNR of 30 dB, both systems achieve a rate of about 14 bits/s/Hz, meaning that FRIS is able to achieve a similar sum-rate performance but with much less number of elements. This also indicates that position reconfigurability of elements can restore the DoF lost by a reduced number of elements, which may have strong practical relevance to RIS technologies.

Fig. 7 evaluates the impact of the number BS antennas in the sum-rate performance for the FRIS-aided MU-MISO system and we provide the rate results against the SNR for different values of $M = 8, 16, 20$. The results demonstrate that the sum-rate improves as the number of BS antennas increases but it does have a diminishing return. This can be explained by the fact that the sum-rate is dictated by the channel rank which is

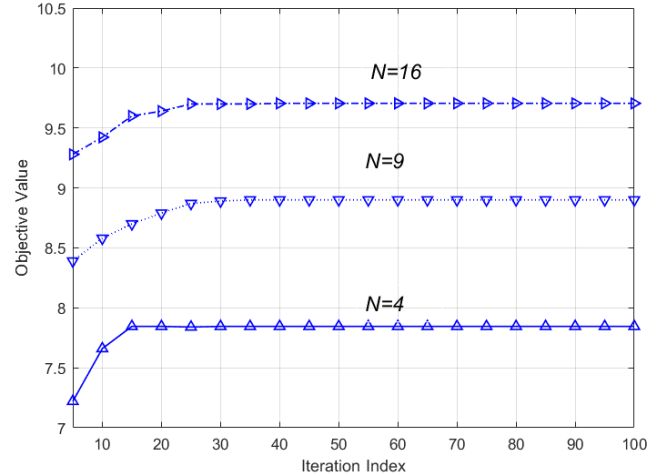


Fig. 5. Convergence performance of Algorithm 1 when SNR is 10 dB.

limited by the fixed number of elements in the FRIS.

Fig. 8 reveals the impact of the size of FRIS on the sum rate assuming SNR = 5 dB and $N = 9$. The results indicate that increasing the area significantly improves the sum rate if FRIS is used while the conventional RIS saturates quickly. This means that even if the number of elements remains the same, there is significant spatial diversity that can be obtained using position reconfigurability. In particular, according to the results in this figure, if the size of FRIS is large enough, it is possible to achieve more than double the sum rate compared to the RIS counterpart, demonstrating the effectiveness of FRIS.

Finally, we use the results in Fig. 9 to study the convergence performance for solving each sub-problem in the optimization of the FRIS-aided MU-MISO system. As can be seen, the proposed algorithms converge very quickly, ensuring that the system converges to an optimal configuration with a smaller number of iterations. Specifically, the phase shift and precoding optimization only need two iterations to converge in each round while the position optimization takes 10 to 15 iterations to reach a steady state. Overall, these results validate the computational feasibility of the proposed alternating optimization framework for optimizing the FRIS network.

V. CONCLUSION

This paper proposed the new paradigm of FRIS-aided wireless communications, where each FRIS element is position-reconfigurable, enhancing the DoF for system optimization. We considered both SU-SISO and MU-MISO models and addressed the achievable rate (or sum-rate) maximization problem. For the SU-SISO scenario, we formulated the problem to obtain the optimal fluid element positions and solved it using a PSO-based approach. We then extended the framework to the MU-MISO case, where FRIS element positions, phase shifts, and BS precoding were jointly optimized in an iterative manner to maximize the system sum-rate. The proposed iterative scheme tackled the joint optimization by decomposing it into three subproblems, which were solved using a combination of grid search, PSO, SDR, and MMSE methods. Numerical

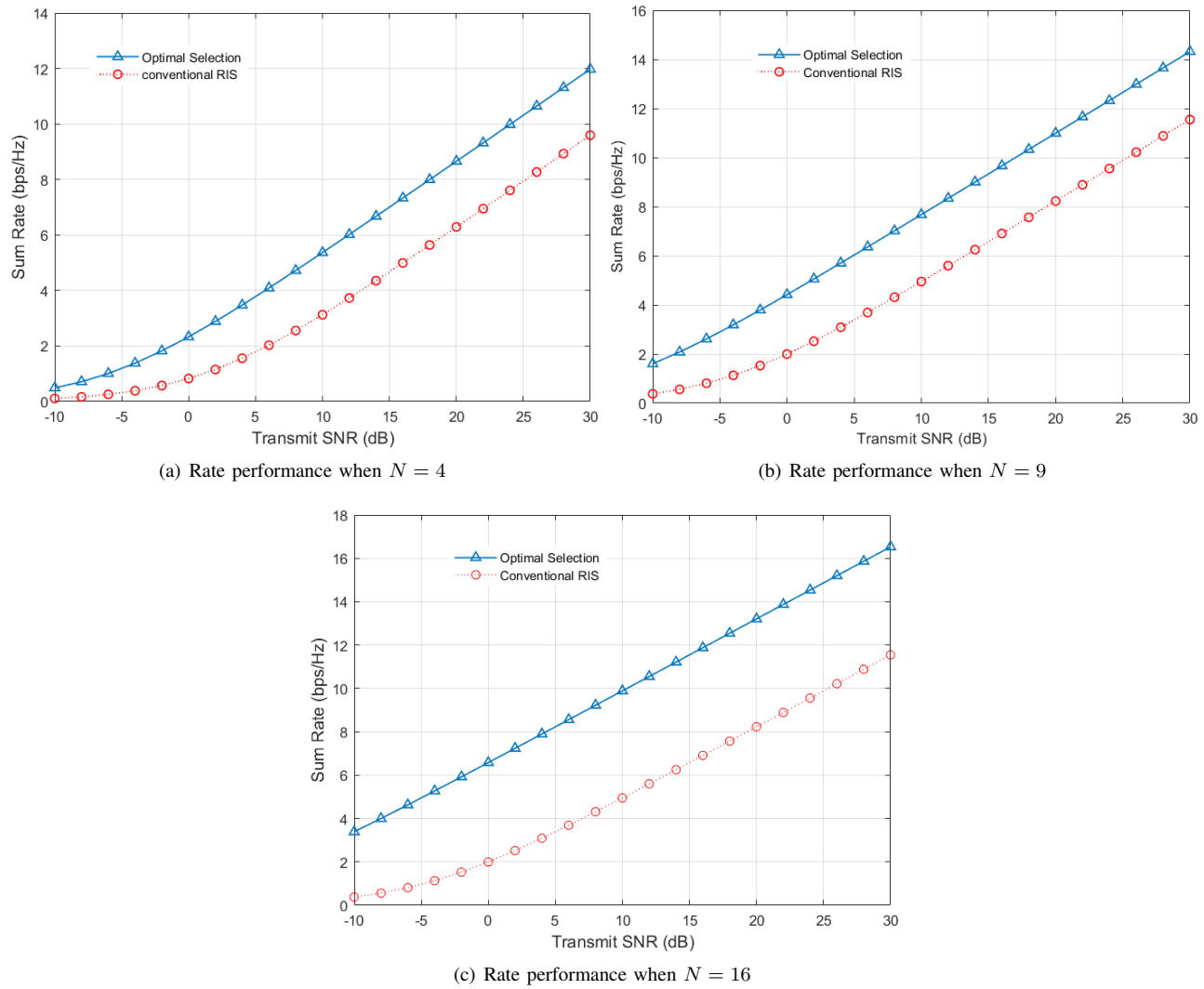


Fig. 6. Comparison between the proposed FRIS-aided MU-MISO and conventional RIS systems.

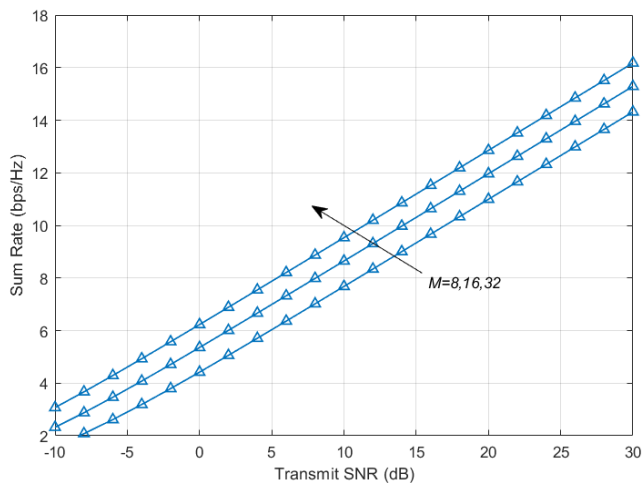


Fig. 7. Sum-rate performance of FRIS-aided MU-MISO against the SNR with different number of BS antennas when $N = 9$.

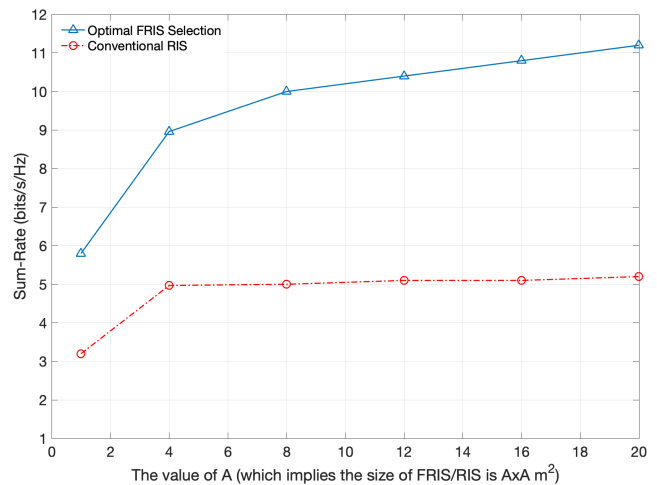


Fig. 8. Sum-rate performance of FRIS-aided MU-MISO against the size of FRIS/RIS when $\text{SNR} = 5$ dB and $N = 9$.

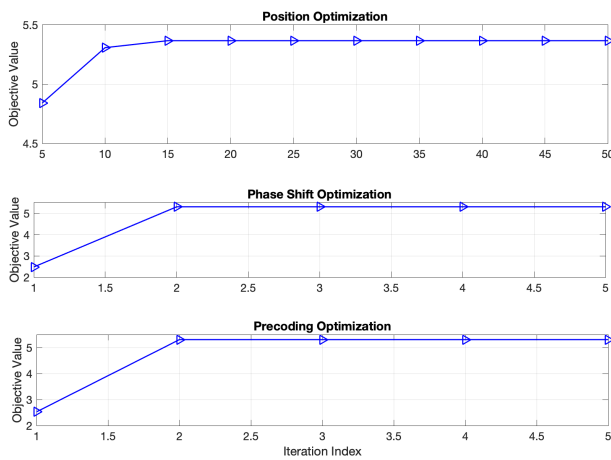


Fig. 9. Convergence performance of each sub-problem of Algorithm 3 when there are $N = 4$ fluid elements and the SNR is 10 dB.

results demonstrated that FRIS significantly outperforms conventional RIS configurations. Notably, FRIS can achieve the same rate with a much smaller number of elements compared to conventional RISs, highlighting its efficiency and potential for next-generation wireless networks.

REFERENCES

- [1] E. Basar, G. C. Alexandropoulos, Y. Liu, Q. Wu, S. Jin, C. Yuen, O. Dobre, and R. Schober, "Reconfigurable intelligent surfaces for 6G: Emerging applications and open challenges," *IEEE Veh. Technol. Mag.*, vol. 19, no. 3, pp. 27–47, Sep. 2024.
- [2] C. Huang, A. Zappone, G. C. Alexandropoulos, M. Debbah, and C. Yuen, "Reconfigurable intelligent surfaces for energy efficiency in wireless communication," *IEEE Trans. Wireless Commun.*, vol. 18, no. 8, pp. 4157–4170, Aug. 2019.
- [3] T. Gong, P. Gavrilidis, R. Ji, C. Huang, G. C. Alexandropoulos, L. Wei, M. Debbah, H. V. Poor, and C. Yuen, "Holographic MIMO communications: Theoretical foundations, enabling technologies, and future directions," *IEEE Commun. Surveys & Tuts.*, vol. 26, no. 1, pp. 196–257, 2024.
- [4] G. C. Alexandropoulos *et al.*, "RIS-enabled smart wireless environments: Deployment scenarios, network architecture, bandwidth and area of influence," *EURASIP J. Wireless Commun. Netw.*, 103, pp. 1–38, Oct. 2023.
- [5] G. C. Alexandropoulos and E. Vlachos, "A hardware architecture for reconfigurable intelligent surfaces with minimal active elements for explicit channel estimation," *Proc. IEEE Int. Conf. Acoustics, Speech, and Signal Process.*, Barcelona, Spain, May 2020, pp. 9175–9179.
- [6] G. C. Alexandropoulos, N. Shlezinger, I. Alamzadeh, M. F. Imani, H. Zhang, and Y. C. Eldar, "Hybrid reconfigurable intelligent metasurfaces: Enabling simultaneous tunable reflections and sensing for 6G wireless communications," *IEEE Veh. Technol. Mag.*, vol. 19, no. 1, pp. 75–84, Mar. 2024.
- [7] R. Long, Y.-C. Liang, Y. Pei, and E. G. Larsson, "Active reconfigurable intelligent surface-aided wireless communications," *IEEE Trans. Wireless Commun.*, vol. 20, no. 8, pp. 4962–4975, Aug. 2021.
- [8] R. Akif Tasci, F. Kilinc, E. Basar, and G. C. Alexandropoulos, "A new RIS architecture with a single power amplifier: Energy efficiency and error performance analysis," *IEEE Access*, vol. 10, pp. 44804–44815, May 2022.
- [9] J. Rao *et al.*, "An active reconfigurable intelligent surface utilizing phase-reconfigurable reflection amplifiers," *IEEE Trans. Microwave Theory & Tech.*, vol. 71, no. 7, pp. 3189–3202, Jul. 2023.
- [10] L. Wei, C. Huang, G. C. Alexandropoulos, C. Yuen, Z. Zhang, and M. Debbah, "Channel estimation for RIS-empowered multi-user MISO wireless communications," *IEEE Trans. Commun.*, vol. 69, no. 6, pp. 4144–4157, Jun. 2021.
- [11] M. Jian, G. C. Alexandropoulos, E. Basar, C. Huang, R. Liu, Y. Liu, and C. Yuen, "Reconfigurable intelligent surfaces for wireless communications: Overview of hardware designs, channel models, and estimation techniques," *Intel. Converged Netw.*, vol. 3, no. 1, pp. 1–32, Mar. 2022.
- [12] V. Jamali, G. C. Alexandropoulos, R. Schober, and H. V. Poor, "Low-to-zero-overhead IRS reconfiguration: Decoupling illumination and channel estimation," *IEEE Commun. Lett.*, vol. 26, no. 4, pp. 932–936, Apr. 2022.
- [13] K. Stylianopoulos and G. C. Alexandropoulos, "Online RIS configuration learning for arbitrary large numbers of 1-bit phase resolution elements," in *Proc. IEEE Int. Workshop Signal Process. Adv. Wireless Commun.*, Oulu, Finland, Jul. 2022.
- [14] A. Salem, K.-K. Wong, and C.-B. Chae, "Impact of phase-shift error on the secrecy performance of uplink RIS communication systems," *IEEE Trans. Wireless Commun.*, vol. 23, no. 7, pp. 7376–7391, Jul. 2024.
- [15] W. Jiang *et al.*, "A joint design for multi-band heterogeneous networks when deploying reconfigurable intelligent surface," *J. Commun. & Netw.*, vol. 24, no. 5, pp. 613–623, Oct. 2022.
- [16] A. Ghaneizadeh, P. Gavrilidis, M. Joodaki, and G. C. Alexandropoulos, "Metasurface energy harvesters: State-of-the-art and their potential for sustainable reconfigurable intelligent surfaces," *IEEE Access*, vol. 12, pp. 160464–160494, Sep. 2024.
- [17] J. Wang *et al.*, "Reconfigurable intelligent surface: Power consumption modeling and practical measurement validation," *IEEE Trans. Commun.*, vol. 72, no. 9, pp. 5720–5734, Sept. 2024.
- [18] F. Saggese, V. Croisfelt, R. Kotaba, K. Stylianopoulos, G. C. Alexandropoulos, and P. Popovski, "On the impact of control signaling in RIS-empowered wireless communications," *IEEE Open J. Commun. Society*, vol. 5, pp. 4383–4399, Jul. 2024.
- [19] W. K. New *et al.*, "A tutorial on fluid antenna system for 6G networks: Encompassing communication theory, optimization methods and hardware designs," *IEEE Commun. Surv. & Tutor.*, doi:10.1109/COMST.2024.3498855, 2024.
- [20] W.-J. Lu *et al.*, "Fluid antennas: Reshaping intrinsic properties for flexible radiation characteristics in intelligent wireless networks?" accepted in *IEEE Commun. Mag.*, 2025.
- [21] Y. Huang, L. Xing, C. Song, S. Wang and F. Elhouni, "Liquid antennas: Past, present and future," *IEEE Open J. Antennas & Propag.*, vol. 2, pp. 473–487, Mar. 2021.
- [22] Y. Shen *et al.*, "Design and implementation of mmWave surface wave enabled fluid antennas and experimental results for fluid antenna multiple access," *arXiv preprint, arXiv:2405.09663*, May 2024.
- [23] X. Gao *et al.*, "Liquid metal-based microfluidic metasurface for controllable electromagnetic wave reflection attenuation," *IEEE J. Electron Devices Society*, vol. 10, pp. 898–906, 2022.
- [24] S. Basbug, "Design and synthesis of antenna array with movable elements along semicircular paths," *IEEE Antennas Wireless Propag. Lett.*, vol. 16, pp. 3059–3062, Oct. 2017.
- [25] L. Zhu and K. K. Wong, "Historical review of fluid antenna and movable antenna," *arXiv preprint, arXiv:2401.02362v2*, 2024.
- [26] M. C. Johnson, S. L. Brunton, N. B. Kundtz, and J. N. Kutz, "Sidelobe canceling for reconfigurable holographic metamaterial antenna," *IEEE Trans. Antennas & Propag.*, vol. 63, no. 4, pp. 1881–1886, Apr. 2015.
- [27] N. Shlezinger, G. C. Alexandropoulos, M. F. Imani, Y. C. Eldar, and D. R. Smith, "Dynamic metasurface antennas for 6G extreme massive MIMO communications," *IEEE Wireless Communications*, vol. 28, no. 2, pp. 106–113, Apr. 2021.
- [28] L. You, J. Xu, G. C. Alexandropoulos, J. Wang, W. Wang, and X. Gao, "Energy efficiency maximization of massive MIMO communications with dynamic metasurface antennas," *IEEE Trans. Wireless Commun.*, vol. 22, no. 1, pp. 393–407, Jan. 2023.
- [29] J. Zhang *et al.*, "A novel pixel-based reconfigurable antenna applied in fluid antenna systems with high switching speed," *IEEE Open J. Antennas & Propag.*, doi:10.1109/OJAP.2024.3489215, 2024.
- [30] S. Shen, K. K. Wong, and R. Murch, "Antenna coding empowered by pixel antennas," *arXiv preprint, arXiv:2411.06642*, 2024.
- [31] K. K. Wong, A. Shojaefard, K. F. Tong, and Y. Zhang, "Performance limits of fluid antenna systems," *IEEE Commun. Lett.*, vol. 24, no. 11, pp. 2469–2472, Nov. 2020.
- [32] K. K. Wong, A. Shojaefard, K. F. Tong, and Y. Zhang, "Fluid antenna systems," *IEEE Trans. Wireless Commun.*, vol. 20, no. 3, pp. 1950–1962, Mar. 2021.
- [33] M. Khammassi, A. Kammoun, and M.-S. Alouini, "A new analytical approximation of the fluid antenna system channel," *IEEE Trans. Wireless Commun.*, vol. 22, no. 12, pp. 8843–8858, Dec. 2023.

- [34] J. D. Vega-Sánchez, A. E. López-Ramírez, L. Urquiza-Aguiar, and D. P. M. Osorio, "Novel expressions for the outage probability and diversity gains in fluid antenna system," *IEEE Wireless Commun. Lett.*, vol. 13, no. 2, pp. 372–376, Feb. 2024.
- [35] J. D. Vega-Sánchez, L. Urquiza-Aguiar, M. C. P. Paredes, and D. P. M. Osorio, "A simple method for the performance analysis of fluid antenna systems under correlated Nakagami- m fading," *IEEE Wireless Commun. Lett.*, vol. 13, no. 2, pp. 377–381, Feb. 2024.
- [36] P. D. Alvim *et al.*, "On the performance of fluid antennas systems under α - μ fading channels," *IEEE Wireless Commun. Lett.*, vol. 13, no. 1, pp. 108–112, Jan. 2024.
- [37] C. Psomas, P. J. Smith, H. A. Suraweera, and I. Krikidis, "Continuous fluid antenna systems: Modeling and analysis," *IEEE Commun. Lett.*, vol. 27, no. 12, pp. 3370–3374, Dec. 2023.
- [38] W. K. New, K. K. Wong, H. Xu, K. F. Tong and C.-B. Chae, "Fluid antenna system: New insights on outage probability and diversity gain," *IEEE Trans. Wireless Commun.*, vol. 23, no. 1, pp. 128–140, Jan. 2024.
- [39] W. K. New, K. K. Wong, H. Xu, K. F. Tong, and C.-B. Chae, "An information-theoretic characterization of MIMO-FAS: Optimization, diversity-multiplexing tradeoff and q -outage capacity," *IEEE Trans. Wireless Commun.*, vol. 23, no. 6, pp. 5541–5556, Jun. 2024.
- [40] H. Xu *et al.*, "Channel estimation for FAS-assisted multi-user mmWave systems," *IEEE Commun. Lett.*, vol. 28, no. 3, pp. 632–636, Mar. 2024.
- [41] W. K. New *et al.*, "Channel estimation and reconstruction in fluid antenna system: Oversampling is essential," *IEEE Trans. Wireless Commun.*, vol. 24, no. 1, pp. 309–322, Jan. 2025.
- [42] B. Xu, Y. Chen, Q. Cui, X. Tao and K. K. Wong, "Sparse Bayesian learning-based channel estimation for fluid antenna systems," *IEEE Wireless Commun. Lett.*, doi:10.1109/LWC.2024.3500218, 2024.
- [43] Z. Zhang, J. Zhu, L. Dai, and R. W. Heath Jr, "Successive Bayesian reconstructor for channel estimation in fluid antenna systems," *IEEE Trans. Wireless Commun.*, doi:10.1109/TWC.2024.3515135, 2024.
- [44] Z. Chai, K. K. Wong, K. F. Tong, Y. Chen, and Y. Zhang, "Port selection for fluid antenna systems," *IEEE Commun. Lett.*, vol. 26, no. 5, pp. 1180–1184, May 2022.
- [45] L. Zhang, H. Yang, Y. Zhao and J. Hu, "Joint port selection and beamforming design for fluid antenna assisted integrated data and energy transfer," *IEEE Wireless Commun. Lett.*, vol. 13, no. 7, pp. 1833–1837, Jul. 2024.
- [46] C. Wang *et al.*, "Fluid antenna system liberating multi-user MIMO for ISAC via deep reinforcement learning," *IEEE Trans. Wireless Commun.*, vol. 23, no. 9, pp. 10879–10894, Sept. 2024.
- [47] L. Zhou, J. Yao, M. Jin, T. Wu and K. K. Wong, "Fluid antenna-assisted ISAC systems," *IEEE Wireless Commun. Lett.*, vol. 13, no. 12, pp. 3533–3537, Dec. 2024.
- [48] J. Zou *et al.*, "Shifting the ISAC trade-off with fluid antenna systems," *IEEE Wireless Commun. Lett.*, vol. 13, no. 12, pp. 3479–3483, Dec. 2024.
- [49] K. K. Wong and K. F. Tong, "Fluid antenna multiple access," *IEEE Trans. Wireless Commun.*, vol. 21, no. 7, pp. 4801–4815, Jul. 2022.
- [50] K. K. Wong, K. F. Tong, Y. Chen, and Y. Zhang, "Fast fluid antenna multiple access enabling massive connectivity," *IEEE Commun. Lett.*, vol. 27, no. 2, pp. 711–715, Feb. 2023.
- [51] K. K. Wong, D. Morales-Jimenez, K. F. Tong, and C.-B. Chae, "Slow fluid antenna multiple access," *IEEE Trans. Commun.*, vol. 71, no. 5, pp. 2831–2846, May 2023.
- [52] H. Hong, K. K. Wong, K. F. Tong, H. Shin, and Y. Zhang, "Coded fluid antenna multiple access over fast fading channels," accepted in *IEEE Wireless Commun. Lett.*, 2025.
- [53] K. K. Wong, C.-B. Chae, and K. F. Tong, "Compact ultra massive antenna array: A simple open-loop massive connectivity scheme," *IEEE Trans. Wireless Commun.*, vol. 23, no. 6, pp. 6279–6294, Jun. 2024.
- [54] K. K. Wong, "Transmitter CSI-free RIS-randomized CUMA for extreme massive connectivity," *IEEE Open J. Commun. Soc.*, vol. 5, pp. 6890–6902, Oct. 2024.
- [55] N. Waqar *et al.*, "Opportunistic fluid antenna multiple access via team-inspired reinforcement learning," *IEEE Trans. Wireless Commun.*, vol. 23, no. 9, pp. 12068–12083, Sept. 2024.
- [56] D. Kong *et al.*, "Initial study of a sub-THz reconfigurable reflector using actuated liquid metal droplet," in *Proc. IEEE Int. Symp. Antennas & Propag. & INC/USNC?URSI Radio Sci. Meeting (AP-S/INC-USNC-URSI)*, pp. 2753–2754, 14–19 Jul. 2024, Firenze, Italy.
- [57] J. Ye, P. Zhang, X.-P. Li, L. Huang, and Y. Liu, "Joint beamforming and position optimization for fluid RIS-aided ISAC systems," *arXiv preprint, arXiv:2501.13339v2*, 2025.
- [58] B. Liu, K. F. Tong, K. K. Wong, C.-B. Chae, and H. Wong, "Be water, my antennas: Riding on radio wave fluctuation in nature for spatial multiplexing using programmable meta-fluid antenna," *arXiv preprint, arXiv:2502.04693*, 2025.
- [59] C.-Y. Chiu, C.-H. Cheng, R. D. Murch and C. R. Rowell, "Reduction of mutual coupling between closely-packed antenna elements," *IEEE Trans. Antennas & Propag.*, vol. 55, no. 6, pp. 1732–1738, Jun. 2007.
- [60] A. A. Althwayb *et al.*, "Design technique to mitigate unwanted coupling in densely packed radiating elements of an antenna array for electronic devices and wireless communication systems operating in the millimeter-wave band," *AEU – Int. J. Elect. & Commun.*, vol. 159, no. 154464, Feb. 2023.